Soft Matter

PAPER

View Article Online
View Journal | View Issue

Cite this: *Soft Matter*, 2016, 12, 2766

Nonsolvent-assisted fabrication of multi-scaled polylactide as superhydrophobic surfaces†

Yafang Chang,[a] Xuying Liu,[a] Huige Yang,[a] Li Zhang,[a] Zhe Cui,[a] Mingjun Niu,[a] Hongzhi Liu*[b] and Jinzhou Chen*[a]

Received 12th January 2016,
Accepted 24th January 2016

DOI: 10.1039/c6sm00079g

www.rsc.org/softmatter

The solution-processing fabrication of superhydrophobic surfaces is currently intriguing, owing to high-efficiency, low cost, and energy-consuming. Here, a facile nonsolvent-assisted process was proposed for the fabrication of the multi-scaled surface roughness in polylactide (PLA) films, thereby resulting in a significant transformation in the surface wettability from intrinsic hydrophilicity to superhydrophobicity. Moreover, it was found that the surface topographical structure of PLA films can be manipulated by varying the compositions of the PLA solutions. And the samples showed superhydrophobic surfaces as well as high melting enthalpy and crystallinity. In particular, a high contact angle of 155.8° together with a high adhesive force of 184 μN was yielded with the assistance of a multi-nonsolvent system, which contributed to the co-existence of micro-/nano-scale hierarchical structures.

Introduction

The construction of micro- or nano-structures by mimicking the water-repellent roughness of lotus leafs and rose petals instead of using low surface energy materials (like fluorine-containing polymers) to impart a surface superhydrophobic nature in recent years, has been of considerable interest.[1–7] Basically, this transformation requires a precise regulation of the surface topography through employing complicated processing methods, such as plasma process[8] and template method,[9] in order to significantly enhance the superhydrophobic properties. On the other hand, simple solution processing techniques, including coating,[10] sol–gel process,[11] and spraying,[12] have also been developed for the same purpose, which allow various polymer materials with defined structures to be fabricated and to construct superhydrophobic surfaces; for example, porous polypropylene (PP) prepared by solution deposition onto the substrates was reported to exhibit a high contact angle (CA) of even up to 160°.[13]

In principle, the superhydrophobic surface achieved by solution casting intrinsically originates from phase separation, which results in the aggregation of polymer molecules once the solvent starts to evaporate.[14] It is worth noting that the spatial configuration of the aggregates can be manipulated by introducing nonsolvents.[15] Typically, when polymethylmethacrylate (PMMA) was treated with a nonsolvent, micro- and nano-scale hierarchically porous structures were produced, thereby rendering the coated substrate superhydrophobic,[16] while porous structures with controllable morphologies can be obtained on the surfaces of PMMA microspheres when a nonsolvent having a high surface tension value was used, thereby increasing the CA values from 86.6° (untreated samples) to 145°.[17] Also, superhydrophobic characteristics were observed in other polymer systems, such as polystyrene (PS) and its copolymer, for which the shape-controlled nanoparticles or fibers were indeed formed by either solvent spraying or electro-spinning with the assistance of nonsolvents, ultimately yielding a water-insulated layer with a high CA value of 155°.[18] In addition, the size of the micro-domains induced by phase separation can be adjusted by varying the ratios of solvent/nonsolvent. And when the size of the domains decreased from 7 um to 100 nm, a remarkable increase in CA from 117° to 160° was observed.[6]

As compared to the aforementioned petroleum-based and non-biodegradable polymers that are usually prepared using multiple-step chemical reactions, polylactide (PLA) can be synthesized from renewable resources and also exhibits excellent biodegradability, biocompatibility and mechanical properties and has a broad spectrum of applications, *e.g.*, in food packaging and as electrets.[19–22] Inherently, PLA behaves as a hydrophilic polymer with a water CA of around 80°. So it will be of significant importance to construct superhydrophobic surfaces from these viewpoints to better exploit the potential applications of PLA. However, the formation of superhydrophobic PLA surfaces relies largely on the modification with silica particles[23] or low surface energy substances,[24] because of the good water affinity caused by its characteristic molecular structure.

[a] *School of Materials Science and Engineering, Zhengzhou University, Zhengzhou 450001, China. E-mail: cjz@zzu.edu.cn*
[b] *College of Engineering, Zhejiang Agriculture & Forestry University, Lin'an, Hangzhou, Zhejiang, 311300, China. E-mail: hzliu@iccas.ac.cn*

† Electronic supplementary information (ESI) available: The materials information, preparation process of PLA-i, PLA-ii, PLA-iii, PLA-iv and PLA-v coatings, characterization, thermal and wettability parameters, and images of water droplets on the PLA surface with different tilt angles. See DOI: 10.1039/c6sm00079g

In this contribution, superhydrophobic PLA surfaces were fabricated through a facile process, in which the solvent/nonsolvent dissolution was combined with a solution casting method without any modification of the PLA. Firstly, the pre-coating solutions were prepared through a typical solvent/nonsolvent method described below. Then, the resultant PLA solutions were cast onto glass substrates at room temperature, resulting in the formation of hierarchical surface structures in both micro- and nano-scales. Furthermore, the surface morphologies can be tailored by controlling the solubility and volatilization rate of the solvents. In particular, the effects of different solution concentrations, types of non-solvent as well as pre-drying conditions on the surface morphologies and adhesion properties of resultant PLA coatings were systematically investigated. This work presents a facile and cost-effective route to construct superhydrophobic and biodegradable surfaces.

Experimental

As shown in Table 1, the commonly used aprotic polar chloroform and dichloromethane (DCM), having a similar solubility parameter (SP) to PLA, were chosen as solvents; absolute ethyl alcohol, *n*-butyl alcohol, and *n*-butyl acetate exhibit rather different SP values with PLA, which qualify themselves as nonsolvents for PLA.[25] In addition, the multi-nonsolvents were employed to control the volatilization rate of coating solutions so that the roughness of the deposited PLA surfaces can be precisely tuned. All the materials were measured quantitatively and used in each experiment (see the ESI†).

A certain kind of solvent was mixed with a given non-solvent or multiple ones together in a dry beaker and used as a pre-mixed solvent of PLA (Fig. 1a). Known amounts of PLA pellets were added to the above solvent mixture and magnetic stirring was performed at room temperature until the complete dissolution of PLA was achieved (Fig. 1b). Afterwards, different amounts of nonsolvents were added into the abovementioned pre-coating PLA solution and then stirred again (Fig. 1c). The as-obtained homogeneous solutions (2.5 mL) were coated onto the pre-cleaned glass slides (Fig. 1d), followed by pre-drying at room temperature for 12 h either in a ventilated hood or in air with the cover lid. After the glass slides coated with PLA samples were transferred into the oven for further drying at 40 °C for 48 h, thin films were peeled off from the substrates (Fig. 1e) using a simple lift-off process, as illustrated in Fig. 1f.

Results and discussion

Fig. 2a presents the variation of CA values as a function of nonsolvent contents for the PLA film samples prepared in the ventilated hood. For all samples, a similar trend can be observed

Table 1 Solvents and nonsolvents used to prepare PLA coatings

Samples	Solvents	Nonsolvents
PLA-i	Chloroform	Absolute ethyl alcohol
PLA-ii	Chloroform	Absolute ethyl alcohol and *n*-butyl alcohol
PLA-iii	Dichloromethane	Absolute ethyl alcohol
PLA-iv	Dichloromethane	*n*-Butyl alcohol and *n*-butyl acetate
PLA-v	Dichloromethane	Absolute ethyl alcohol, *n*-butyl alcohol and *n*-butyl acetate

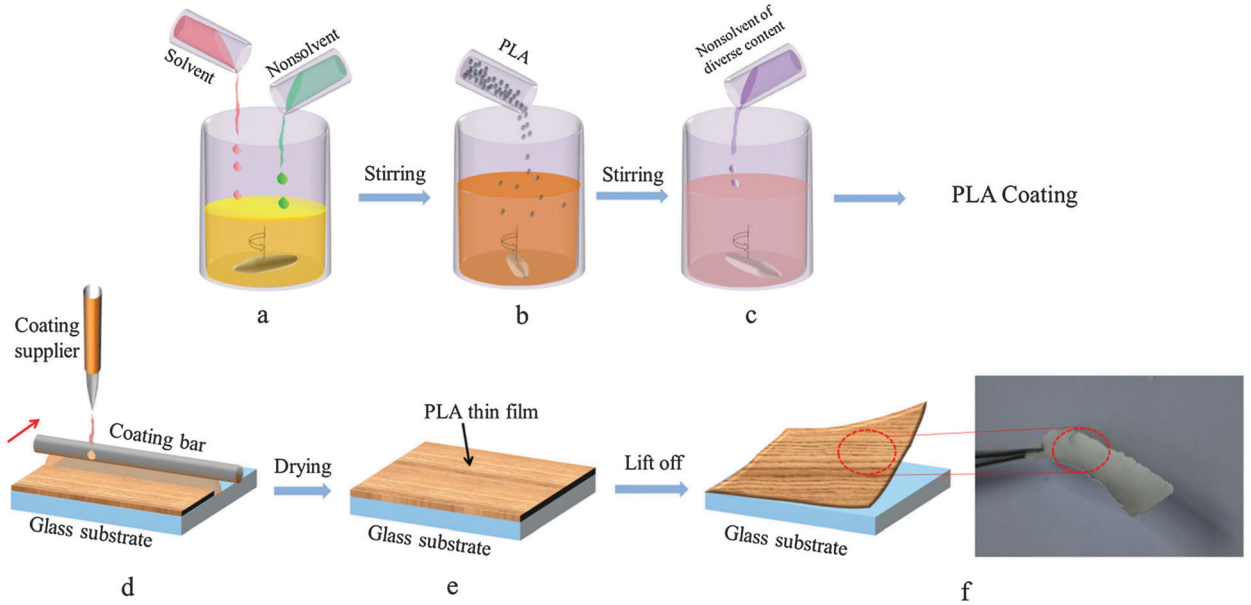

Fig. 1 Schematic fabrication processes of PLA coating (a–c) and its thin films (d–f). Photo image (f) shows the visual appearance of the resultant thin PLA film.

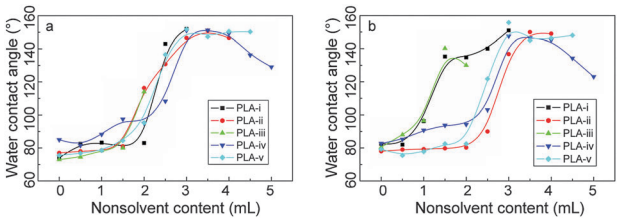

Fig. 2 Dependence of water contact angle values on the content of the nonsolvent under either ventilated hood (a) or the lid covered (b) condition. The volume of pre-coating solution was fixed at 5 mL for each case.

for CA values. Initially, no remarkable change was found in water CA values in the low range of non-solvent content. With further addition of the nonsolvent, the CA values of the resulting films sharply increased until the maximum CA values were attained. The maximum CA values appeared to be 152°, 151°, 151.3°, and 151.8° for the samples of PLA-i, -ii, -iv, and -v, respectively. This suggested that superhydrophobicity was achieved for the samples. But the contents of the nonsolvent at which the maximum CA values were achieved slightly differed for these samples, that is 3, 3.5, 3.5, and 3 mL for PLA-i, -ii, -iii, -iv, and -v, respectively. However, with further increasing the content of the non-solvents, the CA values started to drop. This result could be attributed to the increased aggregate size and loss of film integrity. In Fig. 2b, the sample-v prepared with a cover lid exhibited the highest CA value of more than 155°. Furthermore, the superhydrophobic state became more stable for all the samples. These results indicated that the surface roughness could be improved when the evaporation rate of both the solvent and the nonsolvent was slowed down. With absolute ethyl alcohol as a nonsolvent, the sample PLA-i became superhydrophobic under both evaporation conditions. Comparatively, when the nonsolvent was changed into *n*-butyl alcohol with a low volatilization rate and poor solubility of PLA, the sample PLA-iii did not display superhydrophobic characteristics and its CA value was only 114°. This was due to the fact that fast volatilization rate of DCM in the hood led to a more rapid aggregation and a larger domains size of the PLA molecules. When the lid cover was used, PLA-iii exhibited a higher CA value (140.3°). This result evidenced that a slower evaporation would yield finer micro-domains during the phase separation, thereby improving the water-repellent feature of the PLA films.

Since superhydrophobic properties of the surfaces were largely dependent of their morphologies, both SEM and AFM observations were conducted to examine the surface morphologies of the PLA films. Fig. 3a–j shows the surface morphologies of different PLA film samples. It can be clearly seen from Fig. 3a and b that the sample PLA-i contained many closely packed microspheres. After careful examination, deep grooves and pits in the nanoscale were able to be observed on the surfaces of these spheres. Such hierarchical surface roughness would contribute to the improvement in the hydrophobicity. In Fig. 3c and d, the sample PLA-ii contained similar spherical morphologies to sample PLA-i. But the surface of the former sample appeared more flat and some irregular holes were also present. For the sample PLA-iii (Fig. 3e and f), very smooth spheres with the diameter ranging from hundreds of nanometers to a few microns

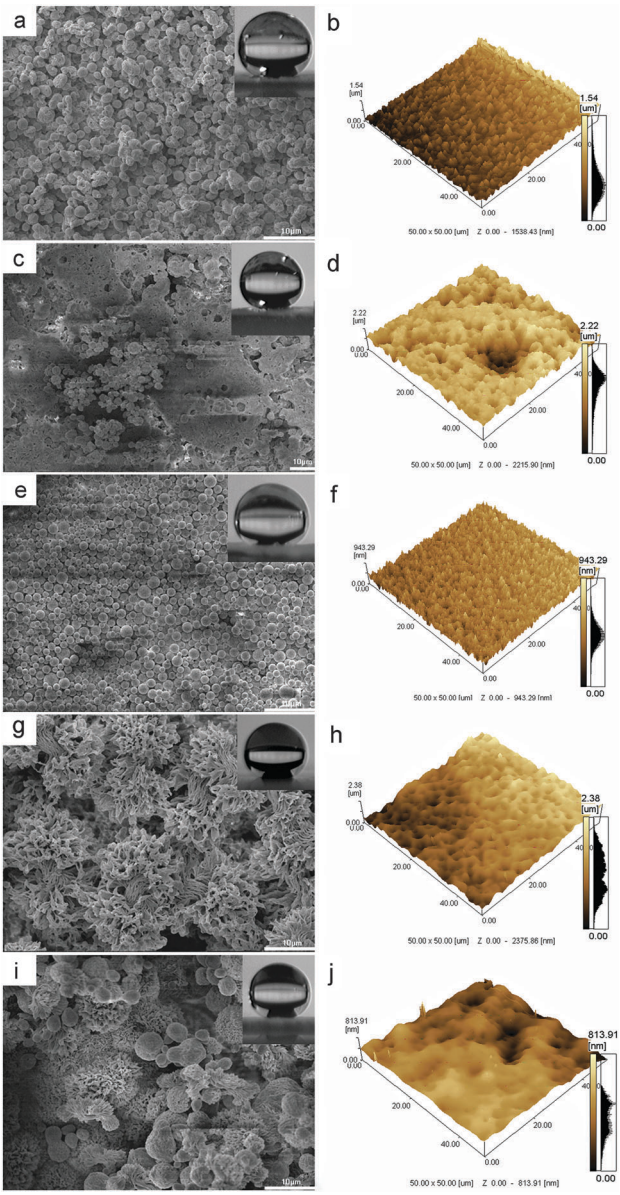

Fig. 3 SEM and AFM images of surface morphologies for the samples: PLA-i (a and b), PLA-ii (c and d), PLA-iii (e and f), PLA-iv (g and h), and PLA-v (i and j). The volume of the pre-coating solution was fixed at 5 mL for each sample, and the content of added nonsolvent was 3 wt% for PLA-i, 3.5 wt% for PLA-ii, 1.5 wt% for PLA-iii, 3 wt% for PLA-iv, and 3 wt% for PLA-v, respectively. The top-right insets of SEM images show a water droplet with a water CA value of 152°, 151°, 140.3°, 151.3°, and 155.8°, respectively (from the top to the bottom).

prevailed in the whole sample. But in this case, the pronounced nanostructure was absent on the surface of these spheres and thus a lower CA value was yielded with respect to the sample PLA-i. As shown in Fig. 3g–j, however, both PLA-iv and PLA-v samples showed quite different surface morphologies from the former ones. The rough surface was characterized by flower-like patterns with the size of about 10 μm. It is worth noting that the surfaces of the flower petals in the sample PLA-iv were also covered with some nano-sized spheres, which may suggest the presence of an intermediate state which is being transformed

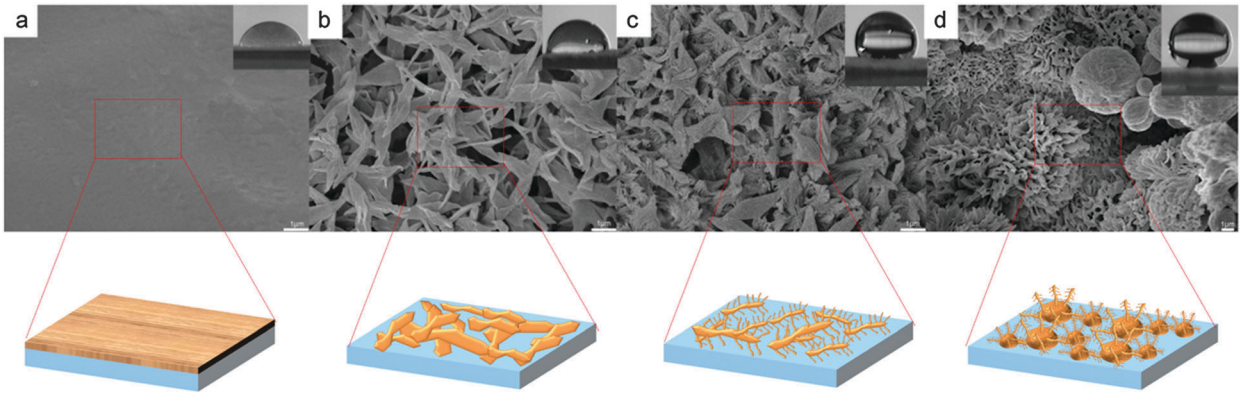

Fig. 4 SEM images and illustrations of surface morphologies for the samples of PLA-v having different CA values. The top-right insets show a water droplet with a contact angle value of 76.8° (a), 92.3° (b), 136.5° (c), and 155.8° (d), respectively.

from spheres to flowers. Since the non-solvents with a higher evaporation rate were employed, the surfaces of sample PLA-v were completely covered by both the flower-like domains with a petal thickness of approximately 100 nm and the microspheres with deep grooves and pits in the nanoscale.

In order to unveil the underlying growth mechanism of the hierarchical structure, the evolution of the surface roughness and the dewetting properties in the sample PLA-v were systematically investigated. As shown in Fig. 4, the surface tended to be superhydrophobic when the nanostructures became dominant. It was clear that a low CA value of 76.8° was observed for the smooth surface (Fig. 4a). When willow leaf-shaped structures appeared, the CA value was slightly increased to 92.3° (Fig. 4b). It was reported that the nanoscale surface structure yielded a high CA value.[13] With further scaling down the domain size of the structural components, a significant increase in the CA value was found, as shown in Fig. 4c. The surface became completely superhydrophobic and had a CA value up to 155.8° when the surface consisted of micro-/nano-scale hierarchical structures (Fig. 4d). Due to the effect of the non-solvent, the surface morphologies of the samples differed from each other. Complex morphologies commonly can be observed in the samples fabricated using multi-nonsolvents. All the surfaces fabricated above consisted of micro-/nano-scale hierarchical structures. These rough structures seem to play an important role in increasing the surface hydrophobicity.

The phase separation caused by the co-use of both the solvent and the nonsolvent, was regarded as the main reason for the formation of unique hierarchical structures and thus the superhydrophobic surface. Fig. 5 depicts the phase separation process. The non-solvent used in this work was miscible with the solvent. Once the PLA resin was dissolved in the mixed solvents, the non-solvent uniformly insulated the PLA molecules. When the PLA solution was coated onto a glass slide, the solvents evaporated more quickly than the non-solvents, and the microphase separation tended to occur. By altering the contents of the nonsolvent in the coating solution, the phase-separation pattern with the micro-/nano-scale hierarchical structure can be obtained in a controlled manner.

When a given amount of a single nonsolvent was added into the pre-coating solution, the nonsolvent mainly acted as a precipitant for PLA (the cases of PLA-i and PLA-iii). Consequently, the homogeneous phase started to separate into two phases: the one consisted of both the solvent and the nonsolvent, while the other designated as the polymer-rich phase containing both the solvent and the PLA. When the ratio of the nonsolvent in the solution increased, the PLA would slowly precipitate out of the solution. The precipitated PLA would act as nuclei and the polymer-rich phase preferred to aggregate around the nuclei in order to lower the surface tension.[14] The reduced amounts of the solvent in the solvent/non-solvent mixture promoted the phase separation, expelling more PLA to precipitate. During the process of phase separation, two phases appeared, *i.e.* the PLA-rich phase and the PLA-poor one. In the polymer-rich phase, the tiny nuclei induced by phase separation gradually developed onto the visible particles as both the solvent and the non-solvent evaporated.[6] Since the non-solvent evaporated more slowly than the solvent, the overall rate of solution evaporation was decreased and the time provided for the particle growth was prolonged, thus yielding larger particles. This would result in the formation of a concentrated PLA phase in the coating solution. As a result, the concentrated PLA phase could form the micro-scale structure, while the less

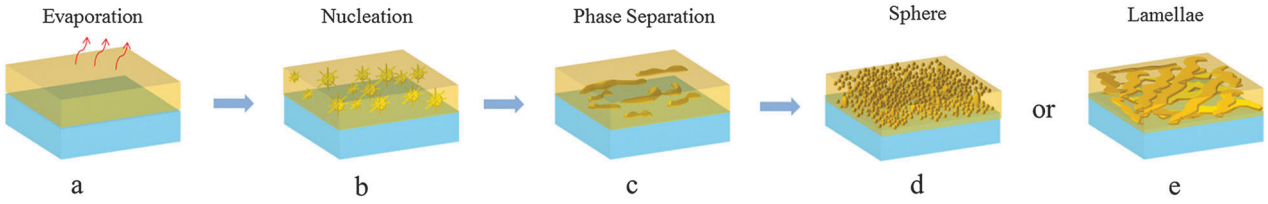

Fig. 5 Schematic preparation processes of PLA coating films.

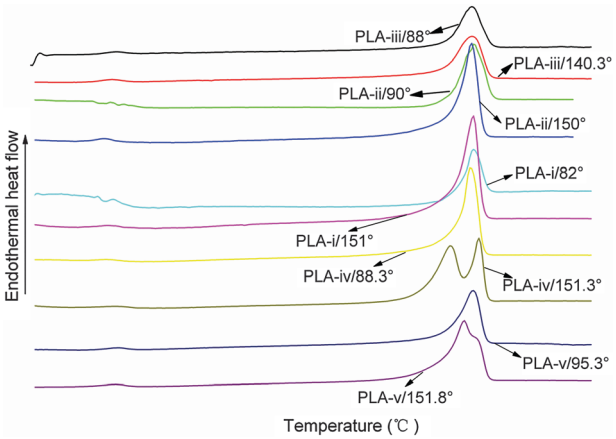

Fig. 6 DSC curves of PLA-i, PLA-ii, PLA-iii, PLA-iv, and PLA-v samples with different CA values at a heating rate of 10 °C min^{-1}.

concentrated PLA phase was responsible for the formation nanoscale structure.

With ethyl alcohol as a nonsolvent, the nucleation of PLA was accelerated and the crystallization time was shortened. The smaller aggregates appeared promptly and further developed into spherulites. Moreover, increasing the ratio of the nonsolvent resulted in the reduced amounts of the solvent in the solvent/nonsolvent phase, thereby resulting in much larger PLA to precipitate. As the boiling point of chloroform and DCM were 61.7 °C and 39.7 °C, respectively, the drying rate of sample PLA-iii was so rapid compared to that of sample PLA-i. This accounted for the observation that the morphology of sample PLA-iii was less complex without the pronounced nanostructure and its CA value was lower than that of sample PLA-i.

The boiling point of absolute ethyl alcohol, *n*-butyl alcohol and *n*-butyl acetate were 57.6 °C, 91 °C and 132 °C, respectively. If the evaporation rate was inappropriate, it can be regulated by using a multiple nonsolvent system, in which the nonsolvent with a high boiling point can be employed. For the sample PLA-ii, PLA-iv, and PLA-v, the used non-solvents volatilized more slowly than the solvent and can migrate toward the surface aggregation regions during the evaporation. Since the nonsolvent was less volatile than the solvent, the rate of evaporation would be lowered and the time needed for aggregation formation was prolonged, thus yielding larger aggregates. When the content of the nonsolvent was appropriate, some of the PLA chains on the surfaces tended to shrink, leading to the formation of aggregates with an irregular appearance. The nonsolvent irregularly gathered on the surfaces of the aggregates and finer morphologies such as sags and crests were formed.

In order to further account for the formation of diverse surface morphologies given above, the degree of PLA crystallinity (X_c) was determined using DSC. As shown in Fig. 6, the PLA-i, PLA-ii, PLA-iii, PLA-iv, and PLA-v samples having two different CA values located at 90° and 150°, respectively, were chosen for the DSC measurement. Various thermal and surface wettability parameters are summarized in Table S1 (ESI†). X_c was calculated on the basis of the melting enthalpy (ΔH_f) value of 100% crystalline PLA being equal to 93.1 J g^{-1}.[26] It can be seen that the contact angle hysteresis (θa–θr) values of samples with CA above 150° were quite high, which demonstrated that the films were superhydrophobic with a high adhesive force like the petal effect. All the samples with a high CA value also exhibited high ΔH_f and X_a values, which may result from a slow crystallization process due to the presence of more nonsolvent. Specially, both PLA-i and PLA-ii samples with a higher CV value showed a much higher X_c, which agreed with the variation trend in Fig. 1a. The sample PLA-iii with a higher CA value also displayed a higher X_c than that with a lower CA one. But the change of X_c with CA values for the sample PLA-iv was not as obvious as that for the other ones. This unique phenomenon was presumably correlated with a new crystal structure as shown in its DSC curve.[27] For the sample PLA-v, the change of X_c was almost the same as the sample PLA-i except a small convex shoulder at the temperature above T_m. The result also demonstrated that the special morphology of the hydrophobic surface relied strongly on the polymer crystallization rate during the solvent evaporation. At higher contents of the non-solvent, the solvent evaporation will be decreased and the polymer crystallization time could be thus prolonged.[28]

Furthermore, the study of wetting states of a droplet on a rough surface would be useful for practical applications. As displayed in Fig. 7, three states can be typically described as the Wenzel state (Fig. 7a), the Cassie–Baxter state (Fig. 7b), and the Cassie impregnating wetting state (Fig. 7c), respectively. When a water droplet was fixed onto the surface of a PLA-v film, it belonged to a classical Wenzel state with a CA value below 150° (Fig. 4a–c). When the content of the nonsolvent was low, the

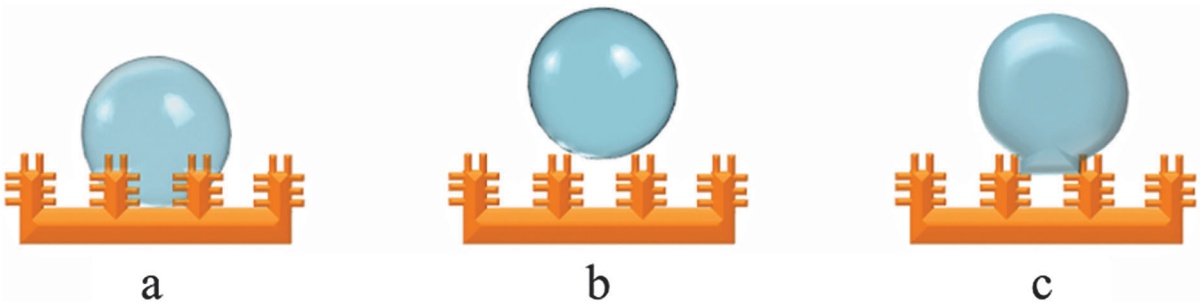

Fig. 7 The wetting states of a droplet on a rough surface: (a) Wenzel wetting state, (b) Cassie–Baxter wetting state, (c) Cassie impregnating wetting state.

surface exhibited the homogeneous wetting with a droplet adhering to the surface. With increasing contents of the nonsolvent, the wetting state transformed into the Cassie impregnating wetting state (Fig. 4d and Fig. S2a) with a CA value of more than 150°, and the droplets were unable to roll off on the surface with the tilted angle of 90° (Fig. S2b) and even hardly dropped down in the case of Fig. S2c (ESI†).

This observation was closely correlated with the surface with a hierarchical roughness which would trap the air to support the water droplet and therefore gave rise to a more hydrophobic surface than the surface with less roughness. For the lotus effect, the droplets can roll off more easily in the Cassie–Baxter state than a flat surface because the capture effect of air in both gaps and interstices caused the formation of additional air–water interfaces.[29] However, in the Cassie impregnating wetting state corresponding to the rose effect, the presence of micro-structures was one of the main reasons for the adherence, the water droplet can wet big gaps among the micro-scale structures. Thus, a large amount of liquid–solid contact surfaces would emerge. Therefore, the surface had a high adhesive force and can pin a water droplet. However, the water cannot wet the nano-scale structure, and a large amount of air was trapped in the porous structure and consequently the formed surface exhibited superhydrophobicity.[30–32] The high water adhesion force produced by the superhydrophobic PLA surfaces can be explicated as follows. First, the hierarchically micro-/nano-scale structures accounted for the superhydrophobicity. And the intrinsic hydrophilic characteristic of PLA situated at the apex of the hierarchical surface made the contact area between water and the interstitial regions become the sites for water pinning, which led to the high water adhesion. This phenomenon was termed as the Cassie impregnating wetting state, previously verified by Feng[31] and Bhushan *et al.*[33,34] As for the flower-like domains consisting of micro-/nanoscale hierarchical structures (Fig. 4d), water droplets were able to enter into larger gaps of the PLA film but not into the smaller ones. The resultant superhydrophobic surface with a high adhesive force can be applied as mechanical hands to transfer water droplets.[35]

Fig. 8 shows the relationship of the force–lamella height for PLA-iv, PLA-v and aluminium (Al). It was noteworthy that the

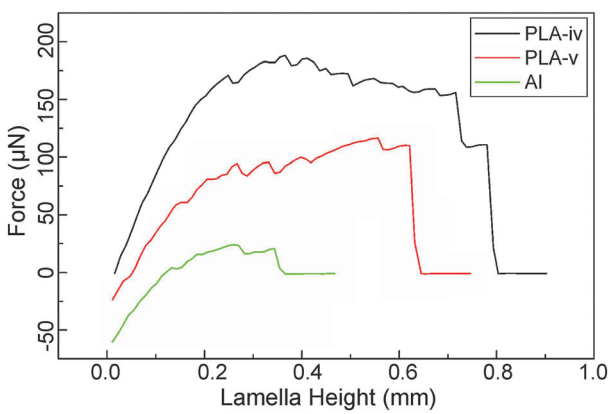

Fig. 8 Force-lamella height of PLA-iv, PLA-v, and aluminium (Al) samples.

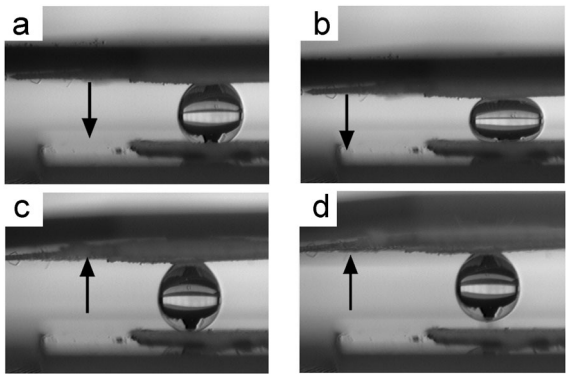

Fig. 9 The demonstration of a liquid droplet transportation from the PLA-v film (Bottom) to the PLA-iv one (Top) at ambient temperature based on the different surface adhesion force between both films.

adhesive force values for PLA-iv and PLA-v samples were equal to 184 μN and 109 μN, respectively, which were much higher than the superhydrophobic Al surface with a CA above 160° for the lotus effect of 22.3 μN. Fig. 9 shows a transportation process of a liquid droplet from the PLA-v film at the bottom to the PLA-iv one at the bottom under ambient temperature. Because of the high adhesive force and superhydrophobic nature of both samples' surfaces, a liquid droplet can be tightly held on the surfaces of both samples without any wetting and sliding during the transportation, which would provide a broad range of application prospect, such as non-loss reversible transport and microfluidic systems.

Conclusions

In this work, we have demonstrated a facile and economical method based on the phase separation induced by the solvent/nonsolvent mixture to construct PLA superhydrophobic surfaces with a high adhesive force. The resultant surfaces exhibited a high water CA of even up to 155.8° and an extremely large adhesion force of 184 μN. It was shown that the phase separation depended on the types and contents of nonsolvents as well as the pre-drying conditions. The observation of the surface morphologies revealed that the hierarchical micro-/nano-scale spheres or the laminated flowers appeared and they were considered to be responsible for the superhydrophobicity of thin PLA films. This work provided a facile and cost-effective method for the fabrication large-area, highly adhesive superhydrophobic PLA surfaces. Such superhydrophobic surfaces would have significant potentials for many applications, such as non-loss transport of microdroplets and anti-icing systems.

Acknowledgements

We thank Prof. Wentao Liu, Prof. Xiaoqing Shen, and Prof. Yukun Liu for their kind help during the experiment. The authors are grateful to the financial supports from the National Natural Science Foundation of China (No. 51573169).

Notes and references

1 N. Blondiaux, E. Scolan, A. M. Popa, J. Gavillet and R. Pugin, *Appl. Surf. Sci.*, 2009, **256s**, s46.
2 H. Li, Y. Zhao and X. Yuan, *Soft Matter*, 2013, **9**, 1005.
3 X. Zhang, N. Zhao, S. Liang, X. Lu, X. Li, Q. Xie, X. Zhang and J. Xu, *Adv. Mater.*, 2008, **20**, 2938.
4 D.-a. Zha, S. Mei, Z. Wang, H. Li, Z. Shi and Z. Jin, *Carbon*, 2011, **49**, 5166.
5 B. N. Sahoo and K. Balasubramanian, *J. Colloid Interface Sci.*, 2014, **436**, 111.
6 U. Cengiz and H. Y. Erbil, *Appl. Surf. Sci.*, 2014, **292**, 591.
7 J. Lv, Y. Song, L. Jiang and J. Wang, *ACS Nano*, 2014, **8**, 3152.
8 Y. P. Li, W. Shi, S. Y. Li and M. K. Lei, *Surf. Coat. Technol.*, 2012, **213**, 139.
9 A. Y. Y. Ho, E. Luong Van, C. T. Lim, S. Natarajan, N. Elmouelhi, H. Y. Low, M. Vyakarnam, K. Cooper and I. Rodriguez, *Colloids Surf., A*, 2014, **52**, 603.
10 I. Yilgor, S. Bilgin, M. Isik and E. Yilgor, *Polymer*, 2012, **53**, 1180.
11 L. Feng, Y. Liu, H. Zhang, Y. Wang and X. Qiang, *Colloids Surf., A*, 2012, **410**, 66.
12 Z. Wu, H. Wang, M. Xue, X. Tian, X. Ye, H. Zhou and Z. Cui, *Compos. Sci. Technol.*, 2014, **94**, 111.
13 H. Y. Erbil, A. L. Demirel, Y. Avcı and O. Mert, *Science*, 2003, **299**, 1377.
14 S. T. Aruna, P. Binsy, E. Richard and B. J. Basu, *Appl. Surf. Sci.*, 2012, **258**, 3202.
15 S. K. Papadopoulou, C. Tsioptsias, A. Pavlou, K. Kaderides, S. Sotiriou and C. Panayiotou, *Colloids Surf., A*, 2011, **387**, 71.
16 J. Gao, J. S. Wong, M. Hu, W. Li and R. K. Li, *Nanoscale*, 2014, **6**, 1056.
17 J. Gao, W. Li, J. S.-P. Wong, M. Hu and R. K. Y. Li, *Polymer*, 2014, **55**, 2913.
18 M. Kang, R. Jung, H.-S. Kim and H.-J. Jin, *Colloids Surf., A*, 2008, **313–314**, 411.
19 A. González and C. I. Alvarez Igarzabal, *Food Hydrocolloids*, 2013, **33**, 289.
20 D. Boonyawan, S. Sarapirom, S. Tunma, C. Chaiwong, P. Rachtanapun and R. Auras, *Surf. Coat. Technol.*, 2011, **205**, S552.
21 Y. Chang, K. Guo, L. Guo, X. Liu, G. Chen, H. Liu, H. Yang and J. Chen, *J. Electrost.*, 2016, **80**, 17.
22 T. Jin and H. Zhang, *J. Food Sci.*, 2008, **73**, 127.
23 G. Y. Bae, J. Jang, Y. G. Jeong, W. S. Lyoo and B. G. Min, *J. Colloid Interface Sci.*, 2010, **344**, 584.
24 P. Pi, W. Mu, G. Fei and Y. Deng, *Appl. Surf. Sci.*, 2013, **273**, 184.
25 S. Sato, D. Gondo, T. Wada, S. Kanehashi and K. Nagai, *J. Appl. Polym. Sci.*, 2013, **129**, 1607.
26 S. Inkinen, M. Hakkarainen, A. C. Albertsson and A. Sodergard, *Biomacromolecules*, 2011, **12**, 523.
27 E. Fukada, *IEEE Trans. Dielectr. Electr. Insul.*, 2006, **13**, 1110.
28 A. L. Ahmad, H. N. Mohammed, B. S. Ooi and C. P. Leo, *J. Polym. Res.*, 2013, **20**, 289.
29 X. M. Li, D. Reinhoudt and M. Crego-Calama, *Chem. Soc. Rev.*, 2007, **36**, 1350.
30 Y. Liu, J. Liu, S. Li, J. Liu, Z. Han and L. Ren, *ACS Appl. Mater. Interfaces*, 2013, **5**, 8907.
31 L. Feng, Y. Zhang, J. Xi, Y. Zhu, N. Wang, F. Xia and L. Jiang, *Langmuir*, 2008, **24**, 4114.
32 R. Hu, G. Jiang, X. Wang, X. Xi and R. Wang, *Bull. Mater. Sci.*, 2013, **36**, 1091.
33 B. Bhushan and E. K. Her, *Langmuir*, 2010, **26**, 8207.
34 B. Bhushan and M. Nosonovsky, *Philos. Trans. R. Soc., A*, 2010, **368**, 4713.
35 J. Huang, Y. Lai, L. Wang, S. Li, M. Ge, K. Zhang, H. Fuchs and L. Chi, *J. Mater. Chem. A*, 2014, **2**, 18531.

